# Room Temperature Ferromagnetism in Cobalt-Doped LiNbO 3 Single Crystalline Films

**ARTICLE** *in* CRYSTAL GROWTH & DESIGN · FEBRUARY 2009

Impact Factor: 4.89 · DOI: 10.1021/cg800754b



**5 AUTHORS**, INCLUDING:

Cheng Song
Tsinghua University
**107** PUBLICATIONS **1,767** CITATIONS
SEE PROFILE

Fei Zeng
Tsinghua University
**186** PUBLICATIONS **3,166** CITATIONS
SEE PROFILE

Article

# Room Temperature Ferromagnetism in Cobalt-Doped LiNbO Single Crystalline Films

Cheng Song, Changzheng Wang, Xuejing Liu, Fei Zeng, and Feng Pan

*Cryst. Growth Des.*, **2009**, 9 (2), 1235-1239• DOI: 10.1021/cg800754b • Publication Date (Web): 05 January 2009



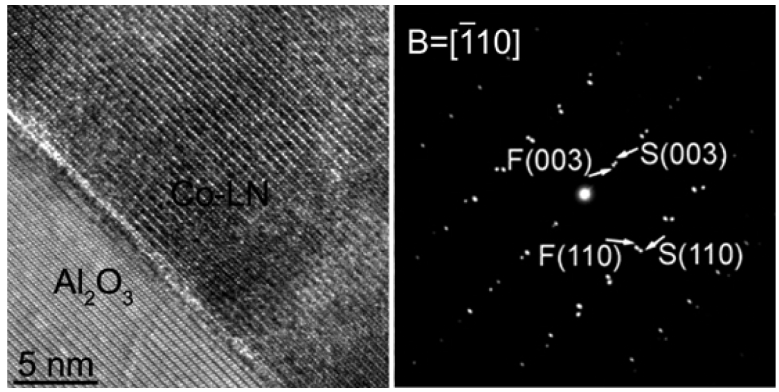


## More About This Article

Additional resources and features associated with this article are available within the HTML version:

- Supporting Information
- Access to high resolution figures
- Links to articles and content related to this article
- Copyright permission to reproduce figures and/or text from this article

View the Full Text HTML

CRYSTAL GROWTH & DESIGN
2009
VOL. 9, NO. 2
1235–1239

# Room Temperature Ferromagnetism in Cobalt-Doped $LiNbO_3$ Single Crystalline Films

Cheng Song,[†] Changzheng Wang,[‡] Xuejing Liu,[†] Fei Zeng,[†] and Feng Pan*[,†]

*Laboratory of Advanced Materials, Department of Materials Science and Engineering, Tsinghua University, Beijing 100084, P. R. China, and Department of Physics, Liaocheng University, Liaocheng City, 252059 Shandong Province, P. R. China*

*Received July 14, 2008; Revised Manuscript Received October 26, 2008*

**ABSTRACT:** Cobalt-doped (5 at. %) $LiNbO_3$ (Co:LN) single crystalline films were prepared by combinatorial laser molecular-beam epitaxy on $Al_2O_3$ (001) substrates. The oxygen atmosphere should be severely controlled to be approximately 10 Pa to obtain stoichiometric Li/Nb concentration. Determined by asymmetric X-ray diffraction and high-resolution transmission electron microscopy, the epitaxial relationship of the sample follows $(003)<100>_F \parallel (003)<100>_S$, $(110)<001>_F \parallel (110)<001>_S$, and $(113)<\bar{1}10>_F \parallel (113)<\bar{1}10>_S$ (F and S denote the film and the substrate, respectively). The Co:LN films have a single-phase, where Co is not metallic but in the 2+ state. Co K-edge X-ray-absorption near-edge structure spectrum determines that $Co^{2+}$ ions substitute for $Nb^{5+}$ lattice sites, producing oxygen vacancies to compensate for the charge nonequilibrium, and shows that the Co−O bond length is greater than that of Co:LN films grown on Si (100) substrates. The Co:LN/$Al_2O_3$ films exhibit a high Curie temperature of ∼550 K and room temperature ferromagnetism of 0.58 $\mu_B$/Co arising from the bound magnetic polarons mechanism based on defects. This work opens a window to a class of single-phase multiferroics by introducing magnetic dopants to ferroelectric materials and to the mechanism of dopants induced ferromagnetism in insulators.

## 1. Introduction

Multiferroic materials that exhibit simultaneous magnetic and ferroelectric ordering are of great interest, both in the fundamental concepts and potential applications.[1−3] However, the coexistence of strong ferromagnetism and ferroelectricity is rarely satisfied in a single phase compound: magnetism and ferroelectricity turn out to be mutually exclusive,[4] and ferromagnets tend to be metallic while ferroelectricity coexists with an insulating state.[2] On the other hand, the research of diluted magnetic semiconductors (DMSs) has determined that the introduction of magnetic ions can dramatically alter the electronic and magnetic properties of the semiconductors. In particular, room temperature ferromagnetism (RTFM) was reported in several transition-metal (TM)-doped oxides, such as ZnO, $TiO_2$, and $SnO_2$.[5,6] It is fundamentally interesting to see whether the achievements in DMSs can be reproduced in the ferroelectric materials, and eventually, to fabricate a class of room temperature single-phase multiferroics.

$LiNbO_3$ (LN) is a well-known and intensively studied ferroelectric crystal, which shows strong room temperature spontaneous polarization of 70 $\mu C/cm^2$, and ferroelectricity of the LN crystal can exist up to a very high ferroelectric transition temperature ($T_E$) of 1483 K.[7,8] Following the idea of the preparation of DMSs,[5,6] RTFM is expected to be introduced to LN by TM doping, as demonstrated in Co-implanted LN wafers.[9] Also, there is a pressing need to grow Co:LN films with highly crystalline quality, which can be used in practical devices, such as waveguide amplifiers/lasers and relevant nonlinear optical devices.[10−12] In this work, film deposition parameters are optimized to obtain Co:LN single crystalline films on $Al_2O_3$ (001) substrates. The films exhibit RTFM of 0.58 $\mu_B$/Co and a high Curie temperature of ∼550 K, which coexists with the dielectric state. The microstructure, local structure, and magnetic property of Co:LN films grown on $Al_2O_3$ (001) and Si (100) substrates are also compared.

## 2. Experimental Details

(5 at.%) Co:LN films (400 nm) were deposited by the combinatorial laser molecular-beam epitaxy (L-MBE) technique.[10] The films were grown on $Al_2O_3$ (001) substrates in various oxygen partial pressures ($P_{O_2}$) of 0.4, 10, and 20 Pa, respectively. The substrate temperature was 700 °C. The film structure and crystalline quality were characterized by X-ray diffraction (XRD). High-resolution transmission electron microscopy (HRTEM), selected area electron diffraction (SAED), and energy-dispersive X-ray spectroscopy (EDS) were used to study the interface bonding and structural characteristics of the films. The valences of constituted element in the Co:LN films were determined by X-ray photoelectron spectroscopy (XPS). X-ray-absorption near-edge structure (XANES) spectra at the Co K-edge were measured in the fluorescence mode using synchrotron radiation. The spectra have been calculated via the full multiple-scattering (MS) theory using the ab initio self-consistent FEFF 8.2 code.[9,13] Magnetization studies were carried out using a superconducting quantum interference device (SQUID) magnetometer at 300 K. High temperature magnetization ($300 < T < 700$ K) was recorded using a vibrating sample magnetometer (VSM) with a magnetic field parallel to the film plane. Induced-coupled-plasma (ICP) measurement was used to determine the composition in the Co:LN films after measuring the magnetic properties.

## 3. Results and Discussion

XRD patterns (the $2\theta$ range is 36−40°) of the Co:LN films in various $P_{O_2}$ of 0.4, 10, and 20 Pa are shown in Figure 1. It is interestingly noted that $P_{O_2}$ has a strong influence on the phase formation in the Co:LN films. The XRD spectrum of the film deposited at the $P_{O_2}$ of 10 Pa only shows the LN (006) reflections, indicating the formation of a stoichiometric Co:LN film. For $P_{O_2} = 0.4$ Pa, the film is Li rich with a peak $Li_3NbO_4$ (222) at $2\theta = 37°$. As $P_{O_2}$ increases to 20 Pa, two phases exist ($LiNbO_3$ and $LiNb_3O_8$), and the film is Li deficient with a peak $LiNb_3O_8$ ($\bar{6}02$) at $2\theta = 38°$. Therefore, the major challenge with the Co:LN growth is the control of the Li species transfer in the plasma from the target to the substrate. Because $Li_3NbO_4$ and $LiNb_3O_8$ phases do not contribute to ferroelectric or electro-

* Corresponding author. Tel.: +86-10-62772907. Fax: +86-10-62771160. E-mail: panf@mail.tsinghua.edu.cn.
[†] Tsinghua University.
[‡] Liaocheng University.

10.1021/cg800754b CCC: $40.75 
Published on Web 01/05/2009

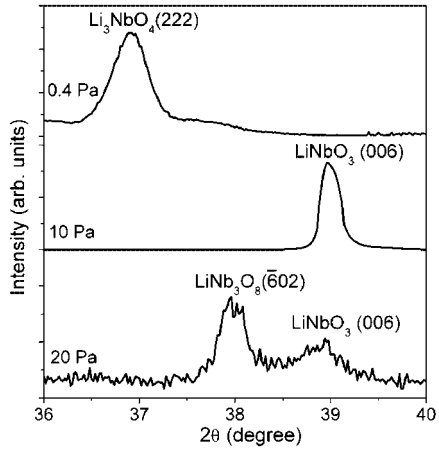


**Figure 1.** XRD patterns (between $2\theta = 36°$ and 40°) of Co:LN/$Al_2O_3$ films prepared at various oxygen atmospheres of 0.4, 10, and 20 Pa.

optic properties,[14] $P_{O_2}$ should be severely controlled to obtain stoichiometric Li/Nb concentration and to grow single-phase Co:LN films.

The phase diagram of the $Li_2O-Nb_2O_5$ system reveals that a complex oxide with Li rich composition is separated into $LiNbO_3$ and $Li_3NbO_4$ domains, and that a complex compound with Li deficient composition is divided into $LiNbO_3$ and $LiNb_3O_8$ domains.[11,12] As the $P_{O_2}$ is low, the formation of $Li_3NbO_4$ phase and the corresponding standard Gibbs energy of formation can be represented by[15,16]

$$Li_2O + LiNbO_3 \rightarrow Li_3NbO_4 \quad (1)$$

$$\Delta G_R^0 = \Delta G_f^0(Li_3NbO_4) - \Delta G_f^0(LiNbO_3) - \Delta G_f^0(Li_2O) \quad (2)$$

where $\Delta G_R^0$ is standard Gibbs energy change for the reaction. On the basis of ref 15 $\Delta G_R^0$ is calculated to be approximately $-195$ kJ mol$^{-1}$ at 700 °C (the substrate temperature). This negative value indicates that the reaction can occur and the $Li_3NbO_4$ phase can appear in the film. On the other hand, when the $P_{O_2}$ is high, the existence of the Li deficient phase $LiNb_3O_8$ can be expressed by[16]

$$Nb_2O_5 + LiNbO_3 \rightarrow LiNb_3O_8 \quad (3)$$

This expression supports the notion that high $P_{O_2}$ is beneficial to the formation of the $LiNb_3O_8$ phase. The appearance of $LiNb_3O_8$ in the high $P_{O_2}$ of 20 Pa in our case is consistent with the previous work that the LN film annealed at the oxygen atmosphere at temperatures higher than 700 °C resulted in the precipitation of the $LiNb_3O_8$ phase, and that rapid thermal annealing could produce transparent and single LN phase film.[14,17]

Figure 2 presents the XRD pattern (between $2\theta = 30°$ and 100°) of the Co:LN film prepared in the $P_{O_2}$ of 10 Pa, in which the two diffraction peaks observed around 38.98° and 81.72° are characteristic of the *R*3*c* LN structure, the *c*-axis being perpendicular to the substrate plane. Very slow scans near the peaks of both hexagonal and cubic cobalt phases reveal no signatures of any kind of additional phases in the film. The sharp and intense peaks observed indicate that the films are highly crystallized, which is further confirmed by asymmetrical XRD. The Φ scan of the film obtained from the (113) planes is displayed in inset a of Figure 2. The peaks are separated by 60°, indicating a 6-fold symmetry of the Co:LN film in the plane. Insets a and b of Figure 2 compares the Φ scan for the

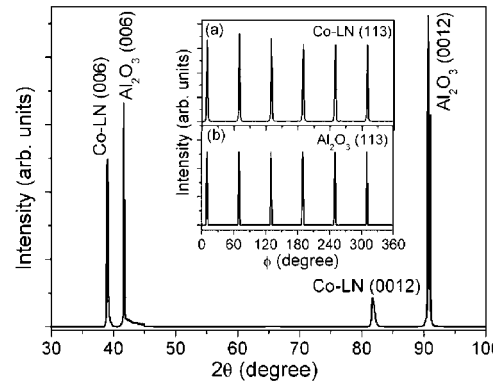


**Figure 2.** XRD pattern of the Co:LN/$Al_2O_3$ film prepared at the oxygen atmosphere of 10 Pa. Insets (a) and (b) show Φ scan of the {113} family peaks of the Co:LN film and the $Al_2O_3$ substrate, respectively.

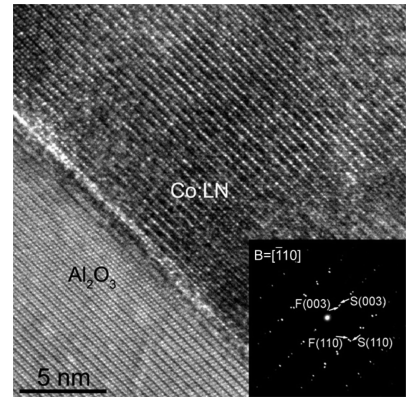


**Figure 3.** Cross-sectional HRTEM image of Co:LN/$Al_2O_3$. The inset is the SAED pattern for the Co:LN/$Al_2O_3$ cross-section.

Co:LN film and the $Al_2O_3$ substrate. Interestingly, a comparison of the peak positions reveals that the epitaxial growth possesses no in-plane rotation between the film and the substrate, indicating that the indices <uvw> of the parallel directions on the parallel planes are the same. This is due to the low lattice mismatch between the Co:LN film ($a = 5.15$ Å, $c = 13.86$ Å) and the $Al_2O_3$ substrate ($a = 4.76$ Å, $c = 12.99$ Å).

HRTEM was performed to investigate the different phases that might have formed in the nanosize range and to determine the orientation relationship between the film and the substrate. The typical cross-sectional HRTEM image of Co:LN/$Al_2O_3$ is depicted in Figure 3. There is no observation for the presence of Co metal (above 6 at. %) or Co-based oxide clusters in the overall of films. In contrast, the doping Co is soluble, that is, homogeneously distributed in LN. EDS data taken at a number of locations throughout the specimens reveal a solid solution of Co dissolved in LN, with Co concentrations ranging from ~4.6−5.3 at. % incorporated into the lattice. From the SAED pattern at the Co:LN/$Al_2O_3$ interface corresponding to the [$\bar{1}$10] zone (the inset of Figure 3) and the asymmetrical XRD patterns, it is determined that the orientation relationship between the Co:LN film and the $Al_2O_3$ substrate is $(003)<100>_F \parallel (003)<100>_S$, $(110)<001>_F \parallel (110)<001>_S$, and $(113)<\bar{1}10>_F \parallel (113)<\bar{1}10>_S$ (F and S denote the film and the substrate, respectively). In contrast to the epitaxial growth of the Co:LN film on the $Al_2O_3$ substrate, Co:LN films deposited on Si (100) substrates with the same preparation parameters behave as

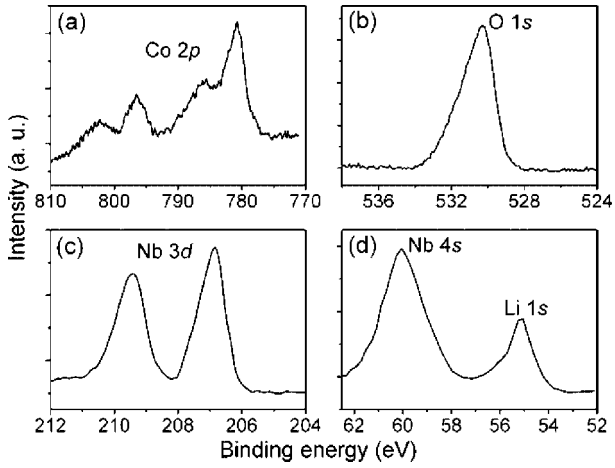


**Figure 4.** Core-level XPS spectra of the constituent elements in the Co:LN film. (a) Co 2*p*. (b) O 1*s*. (c) Nb 3*d*. (d) Li 1*s* and the nearby Nb 4*s* level.

polycrystalline structure.[10] In particular, the former one exhibits a sharp film/substrate interface.

Figure 4 presents the recorded core line XPS spectra of Co 2*p*, O 1*s*, Nb 3*d* and Li 1*s* (with the nearby Nb 4*s* level) in the Co:LN/$Al_2O_3$ film. The Co 2*p* core level photoemission spectrum of the Co:LN film is depicted in Figure 4a. A comparison of the shape and positions of the primary and satellite peaks reflects that there is a good fit between the Co:LN film and the $Co^{2+}$ standard.[18] Co is thus in the 2+ valence state in the Co:LN film. The O 1*s* spectrum (Figure 4b), used here as a reference for simultaneous monitoring the whole measurement, exhibits almost a Gaussian shape with the value of full-width of half-maximum of 1.88 eV. The Nb 3*d* spectrum indicates $Nb^{5+}$ valence without any contribution of lower values, as shown in Figure 4c. Also, one can notice in Figure 4d that the Li 1*s* line remains in a typical $Li^+$ state.[18] It is then concluded that constituent components in the Co:LN film possess stable state and the film exhibits the charge neutralization.

The experimental Co K-edge XANES of Co:LN/$Al_2O_3$ is compared in Figure 5a with the calculated spectra, to elucidate the local structure of Co dopants in the Co:LN film. The calculated spectra were produced by a finite large cluster which contains 197 atoms within a radius of 8 Å sphere from the central Co atom. It is found that two main features of the calculated spectrum from Co replacing central Nb are in the vicinity of those of the experimental ones, marked by A and B in order of increasing photon energy at $E - E_0 =$ 18.2 and 33.8 eV ($E_0 =$ 7708.8 eV), respectively. More interestingly, the introduction of an oxygen vacancy ($V_O$) in the first coordination leads to a broader A and B peaks in the calculated curve, which greatly improves the quality of the fit. In contrast, the main peaks and the tendency of the curve arising from Co substitution at central Li are obviously different from the experimental one. It is hence concluded that Co mainly replaces the Nb sites with $V_O$ compensating the charge nonequilibrium for $Co^{2+}$ replacing $Nb^{5+}$. The Co atoms mainly replacing Nb in the present Co:LN films is totally different from Co substituting for Li in Co-implanted LN wafers.[9] This difference is most likely ascribed to the distinct energy level in L-MBE and ion implantation. The giant energy and the highly nonequilibrium process of ion implantation can lead to Co replace smaller Li sites, whereas Co replace larger Nb in the film prepared by L-MBE. This phenomenon is consistent with the previous

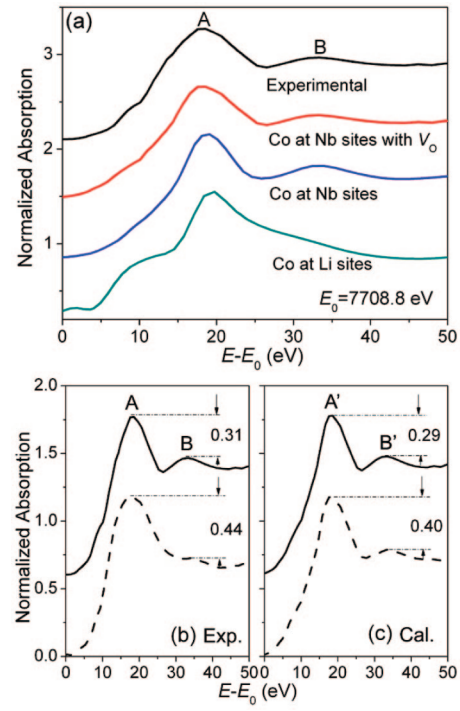


**Figure 5.** (a) Experimental Co *K*-edge XANES spectrum of the Co:LN/$Al_2O_3$ film is compared with the calculated spectra for center Co replacing Nb with and without an oxygen vacancy ($V_O$) in the first coordination as well as Li sites. (b) and (c) are the experimental and MS calculated XANES spectra of Co:LN films grown on $Al_2O_3$ (upper panel) and Si (lower panel) substrates, respectively.

observation that both Nb and Li substitutional sites are possible for a dopant.[19]

Recalling the XRD patterns of the Co:LN films deposited on $Al_2O_3$ (001) and Si (100) substrates,[10] it is noted that Co:LN (006) diffraction peaks are located at 38.98° and 39.26°, respectively, indicating an increase of lattice parameter up to 0.8% and a slight dissimilarity of local Co geometry in Co:LN. Fortunately, XANES and its interpretation are currently of great interest due to its promise of providing local chemical information in complex materials and it is sensitive to ground-state electronic structure.[9,13] The experimental Co K-edge XANES spectra of the Co:LN films grown on $Al_2O_3$ and Si substrates are compared with the ab initio calculated XANES using full MS theory in Figure 5b,c. The lattice location of Co shows trigonal $C_3$ symmetry and lies on a 3-fold axis.[9] The atomic arrangement discrimination among the Co:LN films on the $Al_2O_3$ and Si substrates is the change of Co−O bond length in terms of the lattice parameters induced from XRD results. For the Co:ZnO film deposited on $Al_2O_3$, it is found that Co photoabsorber is surrounded by the first-shell composed of two oxygen atom (and a $V_O$) at 1.936 Å and three oxygen atoms at 2.220 Å, which results in differences of 0.31 and 0.29 between features A and B in normalized absorption for experimental and calculated spectrum, as compared in the upper panel of Figure 5, panels b and c, respectively. For the Co:LN film grown on Si, center Co is surrounded by the first-shell constituted with two oxygen atom (and a $V_O$) at 1.920 Å and three oxygen atoms at 2.199 Å, leading to larger dissimilarities of 0.44 and 0.40 for experimental and calculated spectrum, as shown in the lower panel of Figure 5, panels b and c, respectively. It is thus found that the substrates have a profound influence on the Co−O bond length in the Co:LN films.

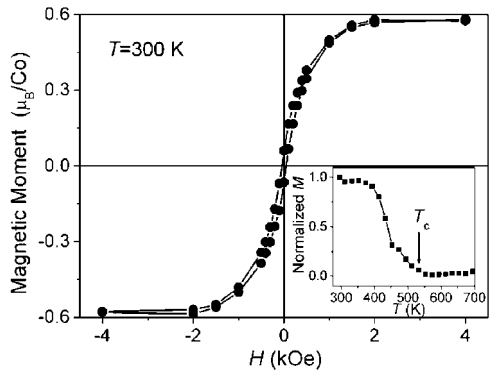


**Figure 6.** Typical magnetic hysteresis loop of the Co:LN/$Al_2O_3$ film measured at 300 K. The inset is the normalized ($M_T/M_{300K}$) $M-T$ curve of the film.

Figure 6 presents a magnetic hysteresis loop of the Co:LN film measured at 300 K in a magnetic field ($H$) up to 4 kOe in a parallel direction to the film layer. It is worth mentioning that the magnetic properties of the $Al_2O_3$ substrate and the pure LN film are measured first with diamagnet-like magnetization, which are subtracted automatically by computer during the measurement of the Co:LN film. From the figure, one sees that the Co:LN film shows obvious RTFM with the magnetic moment of 0.58 $\mu_B$/Co. Also, saturation magnetization is attained at ~2 kOe with a coercive field of 55 Oe. The magnetic moment in the present case is lower than that of Co:LN/Si film (1.2 $\mu_B$/Co). It is also noted that the saturation field is much lower than that of the polycrystalline Co:LN film deposited on Si substrate (~5.5 kOe).[10] The low saturation field and the corresponding high sensitivity of magnetization on magnetic field is worthy of technological consideration.[5]

In general, the ferromagnet should have a high Curie temperature ($T_C$) above 500 K so that it can be used in a wide range of applications without temperature control.[20] The inset of Figure 6 exhibits the ferromagnetic behavior of Co:LN recorded by a VSM for 300 $< T <$ 700 K. Obviously the Co:LN films show ferromagnetism to paramagnetism transitions as the temperature increases.[21] The most interesting result here is that the Co:LN film shows a high $T_C$ of ~550 K, revealing that the Co:LN film possesses promising $T_C$ well above room temperature. As seen from this normalized ($M_T/M_{300K}$) magnetization versus temperature ($T$) curve, the higher temperature (>300 K) magnetization shows a non-Brillouin-like behavior.[22] Such a behavior is theoretically expected in low-carrier density ferromagnets and is suggested to be more typical of insulating ferromagnets. which satisfies the requirements of the existence of ferroelectricity. The Co:LN film grown on semiconducting Si substrate shows ferroelectricity and the resistivity up to ~$10^6$ Ω cm, yet the measurement of the dielectric characteristics of the Co:LN/$Al_2O_3$ film can not be performed because of the lack of conducting bottom electrode ($Al_2O_3$ is dielectric).

RTFM of the Co:LN film can be explained by the interaction between bound magnetic polarons (BMPs) in the case of either low carrier density or equivalently, strong carrier localization.[5,20] The process of film deposition makes it possible that defects (including $V_O$ produced by $Co^{2+}$ replacing $Nb^{5+}$) are located throughout the lattice at arbitrary distances with respect to Co sites. A donor spin of the defects strongly correlates with $Co^{2+}$ within its orbit can mediate effective interactions between them based on a Heisenberg exchange Hamiltonian.[5] Consequently, the donor tends to shape a BMP, coupling $Co^{2+}$ within their orbits. Furthermore, the orbits tend to sufficiently spread out to overlap and interact with adjacent BMPs to realize ferromagnetic ordering.[5] The Co:LN film deposited on the $Al_2O_3$ substrate possesses single crystalline structure and less structural defects than the film grown on Si, corresponding to weaker RTFM. This result is in good agreement with the phenomenon observed by Kaspar et al.[23] that there was a linear relationship between crystalline quality and the magnetic moment and that RTFM arises directly from structural defects. The lower defect density ($\delta$) in the Co:LN/$Al_2O_3$ film leads to a smaller overall volume occupied by BMPs ($\delta\gamma^3$), more isolated $Co^{2+}$ could exist in the film, which makes it hard to realize an effective interaction, leading to lower magnetic moment of the Co:LN/$Al_2O_3$ film.

In addition, XANES spectra have demonstrated that the slight change of Co−O bond length in Co:LN films have a profound influence on the electron movement and scattering in the near range of Co atom. Consequently, electron spin and the corresponding magnetic moments could be sensitive to the Co−O bond length. Different from the scenario in Co:LN/Si system, the longer Co−O bond length promotes ferromagnetism decrease in the Co:LN/$Al_2O_3$ film. This result experimentally supports the prediction obtained by the first principle calculation that the energy differences between ferromagnetic and antiferromagnetic alignment in DMSs are very small.[24,25] A similar phenomenon was observed in Co-doped ZnO films, where a longer Co−O bond length resulted in much weaker RTFM in the films deposited on 64° $Y-X$ $LiNbO_3$ than on 128° $Y-X$ $LiNbO_3$ substrates.[26]

## 4. Conclusion

In summary, Co-doped $LiNbO_3$ single-crystalline films can be prepared in the $P_{O_2}$ of 10 Pa by combinatorial laser molecular-beam epitaxy on $Al_2O_3$ (001) substrates. Lower and higher oxygen atmospheres lead to the formation of Li rich $Li_3NbO_4$ and Li deficient $LiNb_3O_8$ phases, respectively. In the Co-doped $LiNbO_3$ single-crystalline film, $Co^{2+}$ replace $Nb^{5+}$ lattice sites, producing oxygen vacancies to compensate the charge nonequilibrium, and the Co−O bond length is greater than that of the Co-doped $LiNbO_3$ film grown on Si (100). The Co-doped $LiNbO_3$ film grown on $Al_2O_3$ exhibits room temperature ferromagnetism of 0.58 $\mu_B$/Co and a high Curie temperature of ~550 K. The ferromagnetic ordering can be explained by the bound magnetic polarons mechanism based on defects. Less defects in the Co-doped $LiNbO_3$ single-crystalline film lead to the lower magnetic moment in the present case, compared to more robust RTFM observed in Co-doped $LiNbO_3$ polycrystalline films grown on Si. This work demonstrates that room temperature ferromagnetism can be induced in the ferroelectric materials by introducing magnetic dopants, and Co-doped $LiNbO_3$ would open a window to a class of single-crystal multiferroics for device applications at room temperature.

**Acknowledgment.** The authors are grateful to B. He in NSRL for Co-K edge XANES measurements. This work was supported by NSFC (Grant Nos. 50772055 and 50325105).

## References

(1) Fiebig, M. *J. Phys. D: Appl. Phys.* **2005**, *38*, R123–R152.
(2) Eerenstein, W.; Mathur, N. D.; Scott, J. F. *Nature* **2006**, *442*, 759–765.
(3) Ramesh, R.; Spaldin, N. A. *Nat. Mater.* **2007**, *6*, 21–29.

(4) Hill, N. A. *J. Phys. Chem. B* **2000**, *104*, 6694–6709.
(5) Pan, F.; Song, C.; Liu, X. J.; Yang, Y. C.; Zeng, F. *Mater. Sci. Eng., R* **2008**, *62*, 1–35.
(6) Pearton, S. J.; Norton, D. P.; Ivill, M. P.; Hebard, A. F.; Zavada, J. M.; Chen, W. M.; Buyanova, I. A. *J. Electron. Mater.* **2007**, *36*, 462–471.
(7) Inbar, I.; Cohen, R. E. *Phys. Rev. B* **1996**, *73*, 1193–1203.
(8) Zhang, D. L.; Zhang, W. J.; Zhuang, Y. R.; Pun, E. Y. B. *Cryst. Growth Des.* **2007**, *7*, 1541–1546.
(9) Song, C.; Zeng, F.; Shen, Y. X.; Geng, K. W.; Xie, Y. N.; Wu, Z. Y.; Pan, F. *Phys. Rev. B* **2006**, *73*, 172412.
(10) Song, C.; Wang, C. Z.; Yang, Y. C.; Liu, X. J.; Zeng, F.; Pan, F. *Appl. Phys. Lett.* **2008**, *92*, 262901.
(11) Hua, P. R.; Zhang, D. L.; Cui, Y. M.; Wang, Y. F.; Pun, E. Y. B. *Cryst. Growth Des.* **2008**, *8*, 2125–2129.
(12) Zhang, D. L.; Zhuang, Y. R.; Hua, P. R.; Pun, E. Y. B. *J. Appl. Phys.* **2007**, *101*, 013101.
(13) Ankudinov, A. L.; Ravel, B.; Rehr, J. J.; Conradson, S. D. *Phys. Rev. B* **1998**, *58*, 7565–7576.
(14) Akazawa, H.; Shimada, M. *Phys. Status Solidi A* **2006**, *203*, 2823–2827.
(15) Subasri, R.; Sreedharan, O. M. *Solid State Ionics* **1997**, *93*, 341–346.
(16) Cochez, M.; Ferriol, M.; Pöppl, L.; Polgár, K.; Péter, Á. *J. Alloys Comp.* **2005**, *386*, 238–245.
(17) Akazawa, H.; Shimada, M. *J. Mater. Res.* **2007**, *22*, 1726–1736.
(18) Moulder, J. F.; Stickle, W. F.; Sobol, P. E.; Bomben, K. D. *Handbook of X-ray Photoelectron Spectroscopy*; Perkin-Elmer: Eden Prairie, 1992.
(19) Prieto, C.; Zaldo, C.; Fessler, P.; Dexpert, H.; Sanz-García, J. A.; Diéguez, E. *Phys. Rev. B* **1991**, *43*, 2594–2600.
(20) Coey, J. M. D.; Venkatesan, M.; Fitzgerald, C. B. *Nat. Mater.* **2005**, *4*, 173–179.
(21) Chai, P.; Liu, X.; Wang, Z.; Lu, M.; Cao, X.; Meng, J. *Cryst. Growth Des.* **2007**, *7*, 2568–2575.
(22) Das Sarma, S.; Hwang, E. H.; Kaminski, A. *Phys. Rev. B* **2003**, *67*, 155201.
(23) Kaspar, T. C.; Droubay, T.; Shutthanandan, V.; Heald, S. M.; Wang, C. M.; McCready, D. E.; Thevuthasan, S.; Bryan, J. D.; Gamelin, D. R.; Kellock, A. J.; Toney, M. F.; Hong, X.; Ahn, C. H.; Chambers, S. A. *Phys. Rev. B* **2006**, *73*, 155327.
(24) Lee, E. C.; Chang, K. J. *Phys. Rev. B* **2004**, *69*, 085205.
(25) Spaldin, N. A. *Phys. Rev. B* **2004**, *69*, 125201.
(26) Song, C.; Zeng, F.; Geng, K. W.; Liu, X. J.; Pan, F.; He, B.; Yan, W. S. *Phys. Rev. B* **2007**, *76*, 045215.

CG800754B